ELSEVIER

Physica A 244 (1997) 358–369

PHYSICA A

Negative thermal expansion in the Gaussian core model

Frank H. Stillinger*, Dorothea K. Stillinger

Bell Laboratories, Lucent Technologies Inc., Murray Hill, NJ 07974, USA

Abstract

The pressure equation of state of the classical many-body system with Gaussian pair interactions has been examined over a wide density range. Both analytical and simulational methods have been involved. A simply-connected region of negative thermal expansion has emerged from the study. It includes portions of the BCC crystal and fluid sections of the equilibrium phase diagram.

1. Introduction

The occurrence of negative thermal expansion in the liquid phase,

$$\alpha \equiv (\partial \ln V/\partial T)_p < 0\,, \tag{1.1}$$

is an infrequent, but not unique, phenomenon. The case of ordinary water (and its isotopic variants) just above the melting point of ice supplies the best-known example [1]. The example of liquid He^4 just below its λ point [2] demonstrates that the pure elements are not exempt from this behavior. The binary compound In_2Te_3 shrinks upon melting, and continues to shrink during further heating for a substantial temperature range above that melting point [3]. Liquid silica (SiO_2) is easily supercooled, and in that metastable liquid state enters a regime with $\alpha < 0$ [4].

Because these examples are so diverse, it is obvious that several distinct mechanisms can operate to produce negative thermal expansion. Comprehensive understanding of the phenomenon requires examining all such mechanisms. The present paper is devoted to conceptually one of the simplest, arising in the Gaussian core model (GCM) in classical statistical mechanics [5,6]. The appearance of $\alpha < 0$ in the GCM has been pointed out

* Corresponding author. E-mail: fhs@allwise.att.com.

PII S0378-4371(97)00246-X

before [7], but not documented in great detail; providing some of that extra detail and analysis formed the primary motivation for this work.

Section 2 outlines several remarkable mathematical properties possessed by the GCM. These properties strongly influence the equation of state, and produce an unusual phase diagram. Section 3 discusses that phase diagram as it is now understood, based on a combination of analytical and simulational information. Section 4 describes our molecular dynamics investigation of the GCM at five well-separated densities, and identifies the implied $\alpha < 0$ region in the temperature–density plane. Finally, Section 5 contains a discussion of results, including their possible application to selected polymer solutions and suspensions of non-ionic surfactant micelles.

2. Basic mathematical properties

The GCM is defined by its interaction potential Φ. By choosing natural energy and length units, this function adopts the following form for the case of N particles:

$$\Phi(\mathbf{r}_1 \ldots \mathbf{r}_N) = \sum_{i=1}^{N-1} \sum_{j=i+1}^{N} \exp(-r_{ij}^2) . \tag{2.1}$$

No direct attractive forces between pairs of particles are present, so no vapor–liquid phase transition is possible. However, the GCM exhibits crystallization in both two [8,9] and three dimensions [7].

The special character of the Gaussian pair interactions produces several useful mathematical properties. One of these is the possibility to develop high-temperature series for thermodynamic quantities and for particle distribution functions, the individual terms of which are explicit simple functions of density ρ and spatial dimension D [10]. Although these series are formally divergent, they are Borel-summable [11].

Three other basic mathematical properties deserve mention in the present context.

2.1. Hard-sphere limit

This arises from the low-temperature behavior of the pair-interaction Boltzmann factor,

$$B(r, \beta) = \exp[-\beta \exp(-r^2)] , \tag{2.2}$$

where $\beta = (k_B T)^{-1}$. For any $\beta > 0$, B is a monotonically increasing function of r, and for small T (large β) it is useful to locate $r^*(\beta)$, the separation at which B is $\frac{1}{2}$:

$$r^*(\beta) = [\ln(\beta/\ln 2)]^{1/2} . \tag{2.3}$$

At this point, one has

$$[\partial B/\partial r]_{r=r^*} = (\ln 2) r^*(\beta) . \tag{2.4}$$

As $\beta \to +\infty$, so too does r^* and this last derivative. Consequently, B rises very rapidly from essentially zero inside r^* to essentially unity outside r^*, and so r^* plays the role of an effective hard-sphere collision diameter for the GCM. Of course for this hard-sphere connection to apply, it is necessary for the GCM particles to be sufficiently dilute to avoid effective hard sphere close packing:

$$\rho = N/V < 2^{1/2}[r^*(\beta)]^{-3} . \tag{2.5}$$

The well-known properties of the hard-sphere model (both equilibrium and kinetic) hence apply to the low-density, low-temperature limit of the GCM. These include virial coefficients [12], and the coexistence densities of fluid and solid phases [13]. The latter lead to asymptotic estimates, for the GCM at fixed density ρ, of the β values at which the fluid begins to freeze:

$$\beta_{\mathrm{fl}}(\rho) \sim (\ln 2)\exp(0.962\rho^{-2/3}) \tag{2.6}$$

and the FCC crystal begins to melt:

$$\beta_{\mathrm{cr}}(\rho) \sim (\ln 2)\exp(1.027\rho^{-2/3}) . \tag{2.7}$$

Analogous results can be formulated for the two-dimensional hard-disk and GCM systems.

2.2. Convolution property

Define $L(\lambda)$ to be a linear Gaussian-smoothing operator in the DN-dimensional configuration space:

$$L(\lambda) * f = (\pi^{1/2}\lambda)^{-DN} \int \exp[-(\mathbf{R} - \mathbf{R}')^2/\lambda^2] f(\mathbf{R}')\, d^{DN}\mathbf{R} . \tag{2.8}$$

Here λ is the characteristic smoothing length. In particular, we can calculate the smoothed version of the GCM interaction potential:

$$L(\lambda) * \Phi = (1 + 2\lambda^2)^{-D/2} \sum_{i=1}^{N-1} \sum_{j=i+1}^{N} \exp[-r_{ij}^2/(1 + 2\lambda^2)] . \tag{2.9}$$

The effect is to increase the range of the Gaussian pair interactions, while diminishing their strength. The common range increase has the same effect as a uniform compression of the N-particle configuration. Put another way, compressing the GCM uniformly from density ρ to $(1 + \varepsilon)^D\rho$ has the following influence on the potential:

$$\Phi[\mathbf{R}/(1 + \varepsilon)] = (1 + \varepsilon)^D L[(\tfrac{1}{2}\varepsilon^2 + \varepsilon)^{1/2}] * \Phi(\mathbf{R}) . \tag{2.10}$$

Gaussian smoothing $L(\lambda)$ has the effect of diminishing, or even eliminating, features in the function to which it is applied that have length scales smaller than λ. In particular, it can reduce the number of maxima and minima, and can lower the saddle-point-containing barriers between neighboring minima that survive the smoothing. On account

of result (2.10), we can therefore expect that compression will have the effect of washing out the "landscape ruggedness" presented by Φ.

2.3. Duality relations

Owing to the fact that the Gaussian interaction passes into a scaled version of itself under Fourier transformation, it is possible to relate the interaction potential for a Bravais lattice to that of its reciprocal lattice at a dual density [14]. In particular, this permits a many-neighbor lattice sum at high density to be replaced by an equivalent sum at low density where only near-neighbor pairs need to be considered.

Let $\mathbf{b}_1, \mathbf{b}_2$, and $\mathbf{b}_3$ be the basis vectors for the Bravais lattice [15]. The particle number density in this lattice is

$$\rho = |\mathbf{b}_1 \cdot (\mathbf{b}_2 \times \mathbf{b}_3)|^{-1} . \tag{2.11}$$

Basis vectors defining the reciprocal lattice will be denoted by $\mathbf{K}_1$, $\mathbf{K}_2$, and $\mathbf{K}_3$; they are defined by the equations [16]:

$$\mathbf{K}_i \cdot \mathbf{b}_j = 2\pi\delta_{ij} \quad (1 \leqslant i,\ j \leqslant 3) . \tag{2.12}$$

Set I equal to twice the potential energy per particle for one of these lattices, plus one, in the infinite system limit:

$$I = 1 + \lim_{N\to\infty} (2\Phi/N) . \tag{2.13}$$

Then the duality relation states the following identity:

$$\rho^{-1/2} I(\mathbf{b}_1, \mathbf{b}_2, \mathbf{b}_3) = (\rho')^{-1/2} I(\tfrac{1}{2}\mathbf{K}_1, \tfrac{1}{2}\mathbf{K}_2, \tfrac{1}{2}\mathbf{K}_3) . \tag{2.14}$$

Here the relevant dual lattice is not the reciprocal lattice itself, but the version shrunk in each dimension to half its spacing. This shrinkage arises from the length scaling of the Gaussian function under Fourier transformation. The density of this relevant dual lattice is given by the analog of Eq. (2.11):

$$\rho' = |\tfrac{1}{2}\mathbf{K}_1 \cdot (\tfrac{1}{2}\mathbf{K}_2 \times \tfrac{1}{2}\mathbf{K}_3)|^{-1} , \tag{2.15}$$

and along with ρ satisfies the simple relation

$$\rho\rho' = \pi^{-3} . \tag{2.16}$$

Numerical studies [5] reveal that at low density the Gaussian core model has its minimum potential energy in the face-centered cubic lattice arrangement, while at high density the body-centered cubic lattice minimizes potential energy. These constitute a dual lattice pair. Eqs. (2.14) and (2.16) establish that they possess exactly the same

lattice potential energy at the self-dual density

$$\rho = \rho' = \pi^{-3/2} . \tag{2.17}$$

3. Phase diagram

Fig. 1 presents an approximate phase diagram for the single-component, classical Gaussian core model in the T, ρ plane. It is based on a combination of analytical information, and past [7,17,18] and present computer simulation studies. Three stable phases appear, face-centered and body-centered cubic crystals, and isotropic fluid, apparently separated by conventional first-order phase transitions. Note that here and in the following temperature is measured in units of $1/k_B$.

The close-packed FCC crystal is the structure obtained by freezing the hard-sphere system [13], which Section 2.1 above asserts to be the correct low-density limit for the Gaussian core model. Eqs. (2.6) and (2.7) determine the way that the phase boundary curves approach the origin in the T, ρ plane.

The marked decline with increasing density of the melting temperature for the BCC solid is an unusual characteristic of the Gaussian core model. It can be explained in part by the convolution property, Section 2.2 above, which implies a compression smoothing of the potential energy surface in the $3N$-dimensional configuration space. Duality relations, Section 2.3, can be used to estimate the amplitude of variation across the potential energy hypersurface in the high-density limit, from which it follows that the limiting behavior of the melting temperature should be [14]

$$T_m(\rho) \sim C_0 \exp(-C_1 \rho^{2/3}) , \tag{3.1}$$

where C_0 and C_1 are positive constants.

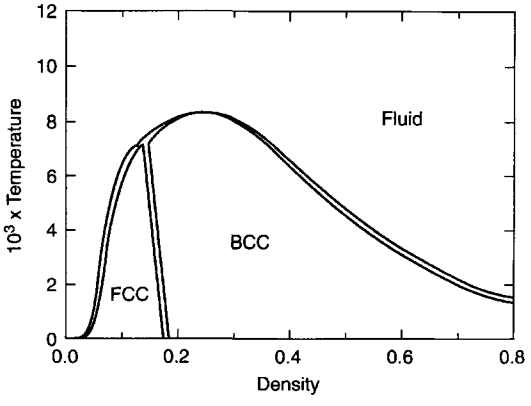

Fig. 1. Approximate phase diagram for the classical Gaussian core model (GCM). The melting-temperature maximum for the BCC crystal is a simple first-order phase change.

With melting temperatures converging to zero in both the low- and high-density limits, at least one melting maximum must exist between those limits. Simulational evidence indicates that it is a single maximum as shown in Fig. 1, at approximate density 0.25, atop the BCC solid region. At this point, coexisting fluid and solid phases have identical densities, but the transition is still first order with a positive latent heat and entropy increase.

The polymorphic transition between FCC and BCC crystals at low temperature spans the self-dual density $\pi^{-3/2}$. No direct information is currently available about the densities at which this transition occurs at high temperatures. However, there is a known tendency for inverse-power-potential models to prefer BCC to FCC at elevated temperature [19]. Therefore, we have somewhat arbitrarily biased the transition to slightly lower density for elevated temperature in the approximate phase diagram in Fig. 1.

4. Molecular dynamics simulations

The following five densities, all above the self-dual density $\pi^{-3/2} = 0.179587\ldots$, have been selected for constant-volume molecular dynamics study of the Gaussian core model:

$$\rho = 0.2, 0.4, 0.7, 1.0, 1.3\,. \tag{4.1}$$

The calculations for the highest density ($\rho = 1.3$) involved 686 particles, while the lower four densities each involved 432 particles. Cubic primitive cells with periodic boundary conditions were used in all cases. Under these conditions the system can attain a perfect BCC structure if the temperature is sufficiently low. Prior molecular dynamics simulations for the Gaussian core model [7,17,18] considered densities 0.2, 0.4, and 1.0; the present work confirms and extends those studies.

In addition to the natural energy and length units that permit Φ to have the simple form Eq. (2.1), we are also free to set particle mass equal to unity. A sixth-order Gear algorithm [20] has been used to integrate the correspondingly reduced form of the Newtonian equations of motion. Reduced time increment $\Delta t = 0.05$ served for all numerical integrations, and for each thermodynamic state examined, a 2000-step equilibration run was followed by a 10 000-step run over which averages were evaluated. In several cases, both heating and cooling state sequences were generated to verify reproducibility of results within expected statistical uncertainty.

By definition, the thermal expansion α, Eq. (1.1), involves a volume (density) change at constant pressure. Our constant-volume simulations detect the sign of α, thanks to the thermodynamic identity

$$\left(\frac{\partial p}{\partial T}\right)_V \left(\frac{\partial T}{\partial V}\right)_p \left(\frac{\partial V}{\partial p}\right)_T = -1 \tag{4.2}$$

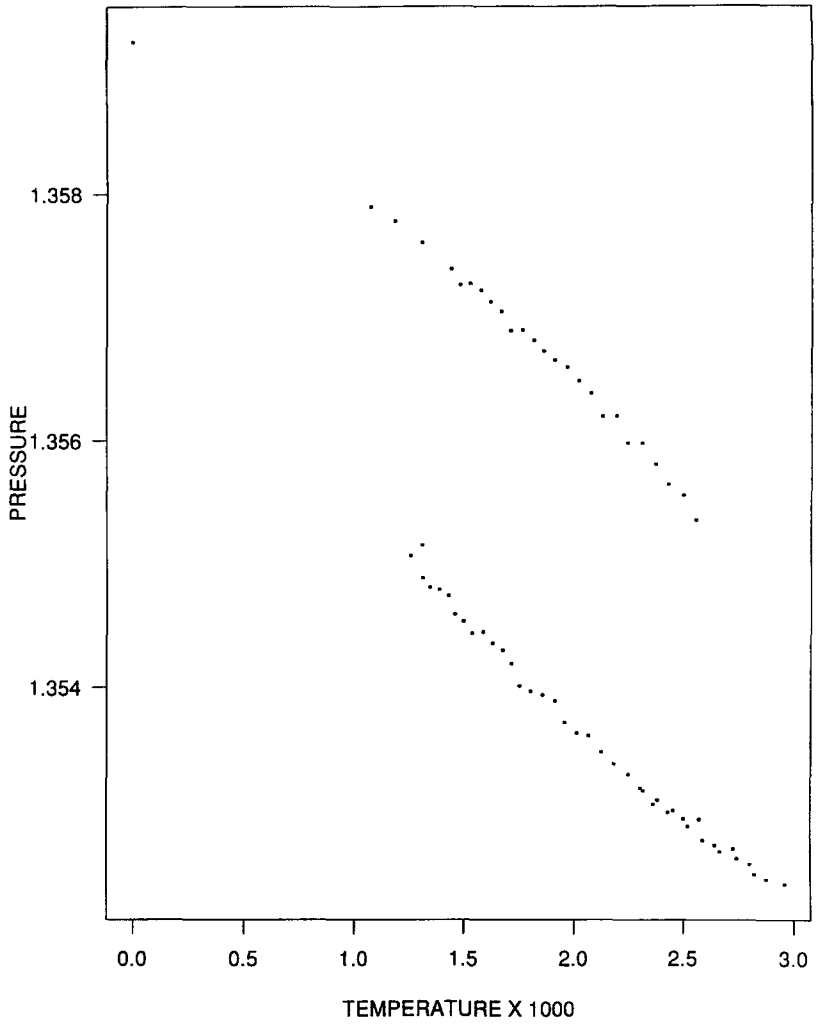

Fig. 2. Virial pressures at $\rho = 0.7$ from the molecular dynamics simulation. The upper branch refers to the BCC crystal, the lower branch to the fluid. Superheated BCC and supercooled fluid extensions are included.

or, equivalently,

$$\alpha = \kappa_T \left(\frac{\partial p}{\partial T} \right)_V , \tag{4.3}$$

where κ_T is the isothermal compressibility that is always positive in a one-phase region. Therefore, the sign of α is the same as that of $(\partial p/\partial T)_V$, a quantity that emerges directly from the simulations.

By way of illustration, Figs. 2 and 3 present virial pressures versus temperature evaluated for the $\rho = 0.7$ case. The first of these shows the low-temperature regime, encompassing both the BCC solid as well as the fluid just above the melting point,

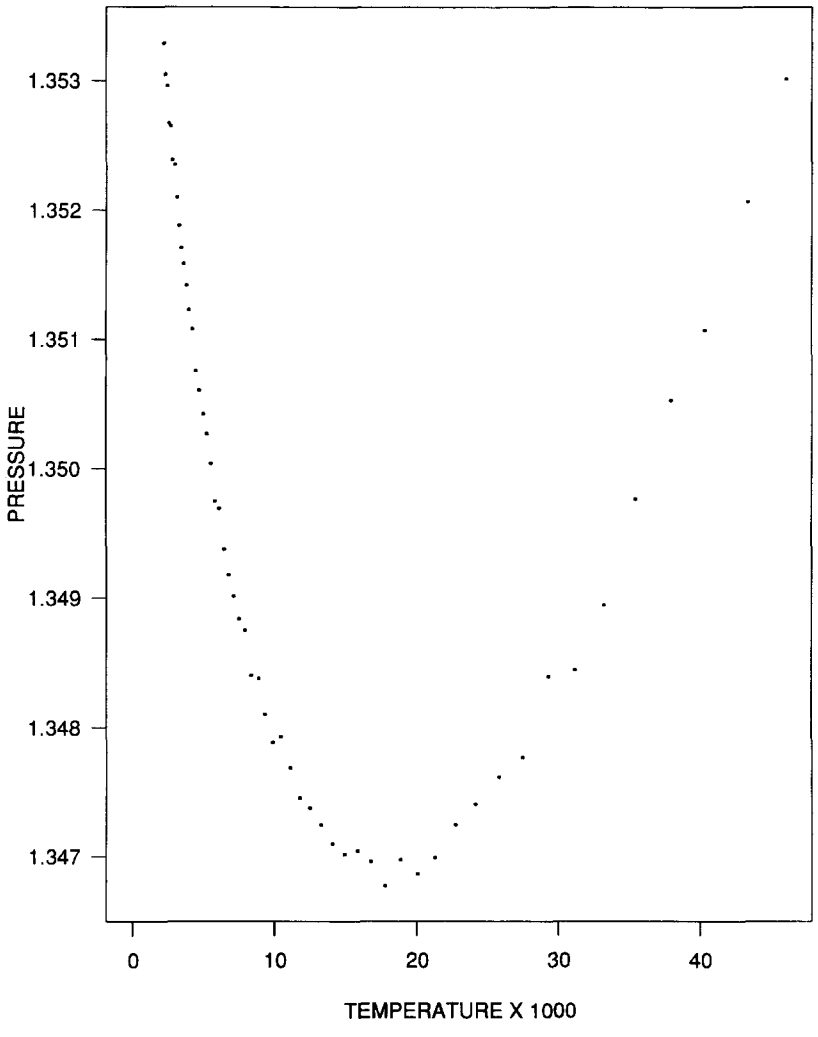

Fig. 3. Fluid-phase virial pressures for the GCM at $\rho = 0.7$ over an extended temperature range, showing a minimum.

demonstrating that both phases have negative α. Fig. 3 involves a considerably wider temperature range, with a pressure minimum and subsequent rise that herald a sign change in α. Similar behaviors (initial pressure decline over BCC and fluid phases followed by a minimum) have been observed for densities 0.4, 1.0, and 1.3; by contrast the system at density 0.2 is "normal" ($\alpha > 0$) at all temperatures, as indicated earlier in Fig. 1.

Table 1 shows the $\alpha = 0$ temperatures $T_{\min}$ that we have determined from the virial pressures, along with several other properties discussed below. It should be recalled that, just as in the case of water and the other substances cited in the Introduction,

Table 1
Selected properties of the Gaussian core model at five densities

ρ	0.2	0.4	0.7	1.0	1.3
$T_{\min}$	—	0.0111	0.0183	0.0170	0.0130
T_{mp}	0.00812	0.00636	0.00197	0.000524	0.000129
$p(0)$	0.0758	0.4235	1.3592	2.7832	4.7050
$p(T_{\min})$	—	0.4200	1.3469	2.7700	4.6926
ϕ_{BCC}	0.152606	0.629311	1.450207	2.284295	3.119429
$\langle\phi_{\mathrm{fis}}\rangle$	0.156883	0.632625	1.451163	2.284523	3.119483

these are temperatures at which the system displays a density maximum when it is examined at fixed pressure. Evidently, densities less than or equal to 0.2 cannot exhibit such density maxima in the Gaussian core model.

Table 1 includes estimates of the melting temperatures T_{mp} for each of the five densities. These were obtained through the Lindemann criterion that identifies melting with attainment of a critical value of the ratio of root-mean-square particle displacement to the nearest-neighbor distance ℓ. For the Gaussian core model this ratio for the BCC crystal has been determined to be [18]

$$\langle(\Delta r_i)^2\rangle/\ell \cong 0.16\,. \tag{4.4}$$

Young and Alder [22] have established that this ratio has the slightly smaller value 0.14 for melting of the FCC hard-sphere crystal, the low-density limiting case of the Gaussian core model discussed in Section 2.1.

Several further quantities are also listed in Table 1 for completeness. These include the pressure in the BCC crystal at absolute zero, $p(0)$, and in the fluid at the minimum, $p(T_{\min})$. Values of ϕ_{BCC}, the $T=0$ crystal potential per particle also appear there. Finally, we have included $\langle\phi_{\mathrm{fis}}\rangle$, mean values of the potential energy per particle for inherent structures (potential energy minima) that are obtained from equilibrium fluid configurations by steepest decent mapping [23–25]; this quantity is substantially independent of the pre-mapping fluid temperature. The convergence to zero with increasing density of the difference

$$\langle\phi_{\mathrm{fis}}\rangle - \phi_{\mathrm{BCC}} \tag{4.5}$$

that is evident from the Table 1 entries clearly illustrates the Φ hypersurface smoothing phenomenon discussed earlier in Section 2.2.

Fig. 4 presents our estimate of the location of the $\alpha<0$ region in the ρ, T plane. It is based on the data shown in Table 1. Both the $T_{\mathrm{mp}}(\rho)$ and $T_{\min}(\rho)$ curves display maxima, but displaced from one another; the former occurs at $\rho\cong 0.25$ while the latter occurs at $\rho\cong 0.75$. We presume that beyond their respective maxima these curves decrease monotonically, approaching zero only as ρ diverges to infinity. Information at present is insufficient to detect a possible discontinuity or other singularity in $T_{\min}(\rho)$

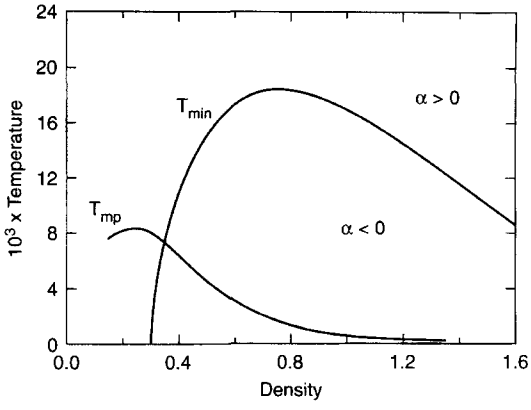

Fig. 4. Estimated region of negative thermal expansion ($\alpha < 0$) for the classical GCM.

as it crosses the BCC-fluid phase boundary, so we have assumed that it is smooth for the purposes of graphical presentation.

5. Discussion

With the exception of liquid He^4, for which strong quantum effects are operative, the liquids with negative α that were mentioned in the Introduction owe their anomalous behavior to the presence of directional bonding interactions. These interactions either directly or indirectly produce open, low-density structures that predominate at low temperature. Thermal motions at elevated temperature cause a partial breakdown and collapse of those open structures, and thus an increase in density at least for a limited temperature range. Similar observations also apply to the case of cubic crystalline ZrW_2O_8 that recently has been shown to possess an isotropic negative thermal expansion over a wide temperature range [26,27].

The Gaussian core model possesses only spherically symmetric pair interactions, Eq. (2.1), so that its region of negative α must stem from a fundamentally different source. The explanation seems to reside in the Φ-hypersurface smoothing induced by compression. Virtually all inherent structures (Φ minima) and their surrounding "basins" converge to a common depth in the asymptotic high-density limit, illustrated specifically by the difference shown earlier in Eq. (4.5). But this requires the higher-lying basins and their boundary-defining barriers to flatten out faster with density increase than do the lower-lying portions of the Φ hypersurface. On average, this means that configurations occurring at higher temperature do not increase in potential energy as rapidly on compression as do the lower temperature configurations. Consequently, the former produce lower pressure than the latter, i.e. $\alpha < 0$.

It has been pointed out before [5] that some polymer solutions, under osmotic solution conditions, might approximate the properties of the Gaussian core model; a similar

remark also apply to solutions of nonionic surfactant solutions. This possible connection arises from the entropic repulsion that can occur between two random polymer coils whose centroids are close enough to permit entanglement, or analogously as amphiphile chains from neighboring micelles interfere. This suggests that negative thermal expansion effects in such systems, observed through temperature and concentration dependence of osmotic pressure, might be attained in real systems as an illustration of this alternative $\alpha < 0$ cause (central forces only).

As a final matter, it should be stressed that the Gaussian core case cannot be unique among central force models in producing a region of negative thermal expansion. The phenomenon is sufficiently strong in the present case that it must survive the addition of at least weak perturbations to the Gaussian pair potentials. In particular, we mention the addition of a weak but long-ranged Kac–Uhlenbeck–Hemmer potential [28],

$$\gamma^3 v(\gamma r_{ij}) , \tag{5.1}$$

for each particle pair. In the limit of vanishing γ this adds a van der Waals term $A\rho^2$ to the pressure, where A may have either sign depending on v, but is independent of T and ρ. Such a term cannot affect the quantity $(\partial p/\partial T)_\rho$ that has been used in the present study to identify the occurrence of negative α, although it might cause a shift in phase boundaries.

References

[1] D. Eisenberg, W. Kauzmann, The Structure and Properties of Water, Oxford University Press, New York, 1969, Ch. 4.
[2] K.R. Atkins, Liquid Helium, Cambridge University Press, Cambridge, 1959, pp. 36–37.
[3] V.M. Glazov, S.N. Chizhevskaya, N.N. Glagoleva, Liquid Semiconductors (A. Tybulewicz, Trans.), Plenum Press, New York, 1969, p. 145.
[4] C.A. Angell, H. Kanno, Science 193 (1976) 1121.
[5] F.H. Stillinger, J. Chem. Phys. 65 (1976) 3968.
[6] D.K. Belashchenko, K.D. Belashchenko, Melts 3 (1990) 105; Russian original version: Rasplavy 3(2) (1989) 32.
[7] F.H. Stillinger, T.A. Weber, J. Chem. Phys. 68 (1978) 3837.
[8] F.H. Stillinger, T.A. Weber, J. Chem. Phys. 74 (1981) 4015.
[9] T.A. Weber, F.H. Stillinger, J. Chem. Phys. 74 (1981) 4020.
[10] F.H. Stillinger, J. Chem. Phys. 70 (1979) 4067.
[11] I.W. Herbst, B. Simon, Phys. Rev. Lett. 41 (1978) 67; see especially footnote 3.
[12] I.C. Sanchez, J. Chem. Phys. 101 (1994) 7003.
[13] W.G. Hoover, F.H. Ree, J. Chem. Phys. 49 (1968) 3609.
[14] F.H. Stillinger, Phys. Rev. B 20 (1979) 299.
[15] N.W. Ashcroft, N.D. Mermin, Solid State Physics, Holt, Rinehart, and Winston, New York, 1976, pp. 64–75.
[16] Ref. [15], pp. 86–94.
[17] F.H. Stillinger, T.A. Weber, J. Chem. Phys. 70 (1979) 4879.
[18] F.H. Stillinger, T.A. Weber, Phys. Rev. B 22 (1980) 3790.
[19] (a) W.G. Hoover, D.A. Young, R. Groves, J. Chem. Phys. 56 (1972) 2207; (b) B.B. Laird, A.D.J. Haymet, Mol. Phys. 75 (1992) 71.
[20] H.J.C. Berendson, W.F. van Gunsteren, in: G. Ciccotti, W.G. Hoover (Eds.), Molecular Dynamics Simulation of Statistical-Mechanical Systems, North-Holland, Amsterdam, 1986, pp. 52–55.

[21] F.A. Lindemann, Phys. Z. 11 (1910) 609.
[22] D.A. Young, B.J. Alder, J. Chem. Phys. 60 (1974) 1254.
[23] F.H. Stillinger, T.A. Weber, Phys. Rev. A 25 (1982) 978.
[24] F.H. Stillinger, T.A. Weber, Science 225 (1984) 983.
[25] F.H. Stillinger, D.K. Stillinger, J. Chem. Phys. 93 (1990) 6013.
[26] T.A. Mary, J.S.O. Evans, T. Vogt, A.W. Sleight, Science 272 (1996) 90.
[27] J.S.O. Evans, Z. Hu, J.D. Jorgensen, D.N. Argyriou, S. Short, A.W. Sleight, Science 275 (1997) 61.
[28] M. Kac, G.E. Uhlenbeck, P.C. Hemmer, J. Math. Phys. 4 (1963) 216.